Dams and Reservoirs under Changing Challenges – Schleiss & Boes (Eds)
© 2011 Taylor & Francis Group, London, ISBN 978-0-415-68267-1

Effects of the Iwate-Miyagi Nairiku earthquake in 2008, Japan, on a central clay core rockfill dam

T. Ohmachi
Japan Dam Engineering Center, Tokyo, Japan

T. Tahara
Tokyo Institute of Technology, Tokyo, Japan

ABSTRACT: The effect of the Iwate-Miyagi Nairiku earthquake in 2008 (*Mj* 7.2), Japan on the Aratozawa dam which is a 74.4 m high rockfill dam with a central clay core is studied with a main focus on the change in the vibration period, shear wave velocity, shear modulus, and pore-water pressure. During the main shock, the acceleration exceeded 10 m/s^2 at the gallery, inducing large shear strains in excess of 10^{-3} and a sudden build-up of the excess pore water pressure in the core. Due to the large strains, the shear wave velocity and shear modulus showed a significant decrease from their initial values and the vibration period was elongated. The full recovery of the wave velocity was found to take at least one year, while the dissipation of the excess pore water pressure seemed faster than the recovery of the wave velocity.

1 INTRODUCTION

The Iwate-Miyagi Nairiku earthquake (*Mj* 7.2) occurred at 8:43 on June 14, 2008 under southwestern Iwate Prefecture, Japan (Japan Meteorological Agency 2008). The Aratozawa dam which is a 74.4 m high rockfill dam constructed mainly for irrigation and flood control purposes, is located 15 km south of the epicenter of the main shock.

During the main shock, strong motion accelerometers installed at the Aratozawa dam registered a peak acceleration of 10.24 m/s^2 at the bottom gallery. Despite such a high acceleration, the dam continued to be in a safe and stable condition for operation because of little damage only. At the dam, the earthquake motion acceleration has been well recorded not only during the main shock of the 2008 earthquake but also during smaller earthquakes before and after the main shock. The total number of the observed earthquakes used in the present study is 189 which consisted of 3 in 1996, 172 in 2008, and 14 in 2009. Table 1 shows

Table 1. Examples of 10 earthquakes out of 189 used in the present study.

No	Date (time)	Magnitude (*Mj*)	Peak acceleration at gallery (m/s^2)
1	1996.8.11 (3:12)	5.9	0.28
2	1996.8.11 (8:10)	5.7	0.33
3	1996.8.11 (15:01)	4.8	0.30
4	2008.6.14 (8:43)	7.2	10.24
5	2008.6.14 (9:00)	4.7	0.99
6	2008.6.14 (9:01)	4.0	4.82
16	2008.6.14 (12:10)	4.7	0.79
19	2008.6.14 (19:11)	4.1	2.29
183	2009.7.1	3.2	0.02
189	2009.8.4	1.6	0.02

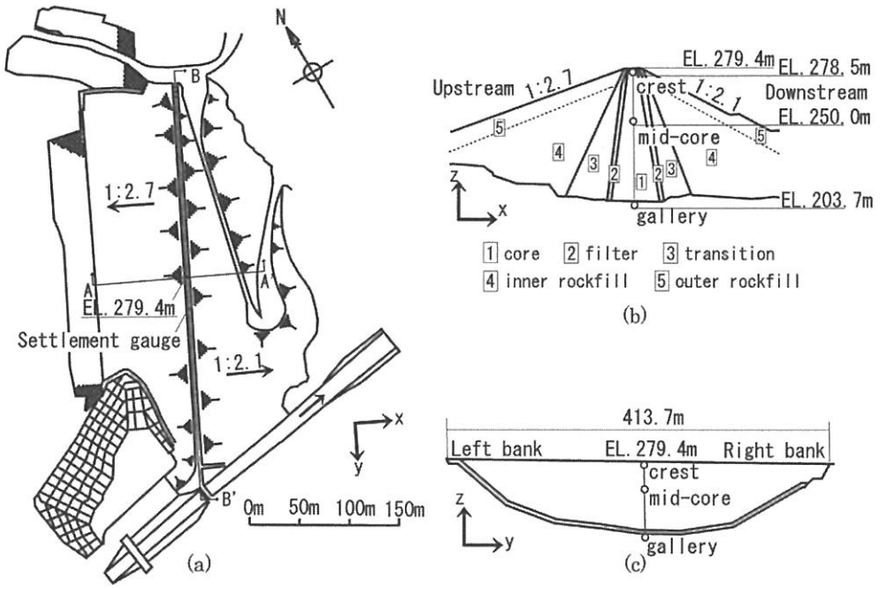

Figure 1. (a). Plan, (b). Cross section A-A' and (c). Cross section B-B' of the Aratozawa dam with seismometers located at crest, mid-core and gallery. Arrows with x, y and z indicate positive directions of observed accelerations.

10 selected earthquakes out of the 189, where all recorded earthquakes used in the present study are numbered from 1 to 189 in chronological order (year/month/day).

2 MAIN FEATURES OF ARATOZAWA DAM AND RESIDUAL DISPLACEMENTS DUE TO THE MAIN SHOCK

The plan and cross sections of the Aratozawa dam are shown in Figure 1. The dam has a central clay core and side slopes of 1:2.7 and 1:2.1 on the upstream and downstream sides, respectively. The seismic coefficient method with a horizontal coefficient of 0.15 was used for the seismic design of the dam. Embankment work of the dam body which was nearly complete in 1991, was followed by construction of appurtenant structures and impounding tests, and the dam was finally completed in 1998. The dam has a crest length of 413.7 m, a crest width of 10 m and the dam body consists of the 5 zones; core, filter, transition, inner rockfill, and outer rockfill zones.

Due to the main shock of the 2008 earthquake, the dam underwent large residual displacements. The residual displacements at the crest shoulder evaluated from the difference between the original design and the survey conducted after the main shock, was 19.8 cm settlement, 4.3 cm towards the upstream, and 6.0 cm to the left at the middle cross section. In the meantime, the top of a plastic pipe of a differential settlement gauge whose location is indicated in Figure 1(a), was observed protruding about 40 cm. According to the measurements of the settlement gauge, the top gauge at EL.275 m showed a settlement of 37.9 cm due to the main shock, which was consistent with the observation of the protruding pipe. In addition, minor cracks in the asphalt pavement were also observed at the right bank corner of the crest.

3 STRONG MOTION RECORDS

Three-component strong motion seismometers (accelerometers) are installed at three locations, i.e. the dam crest, mid-core and bottom gallery (see Fig. 1). The acceleration time histories of the main shock are shown in Figure 2. The peak accelerations observed during the main shock are also shown in Figure 2 where it is seen that, in each direction, the peak

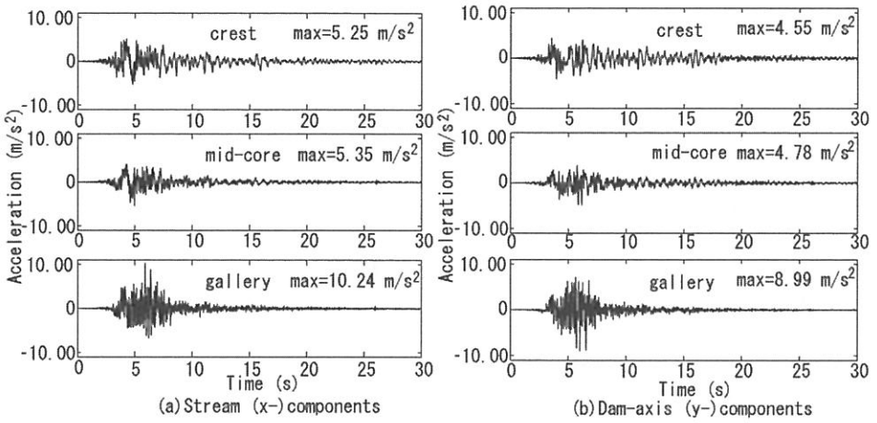

Figure 2. Acceleration time histories of the main shock.

acceleration at the bottom gallery was the largest among the three locations. This fact seems unusual, because earthquake acceleration at a dam crest is usually the largest due to amplification effects of the dam body. The acceleration time histories were sampled at 100 Hz with a frequency range of 0.1–30 Hz and a dynamic range of ±10 m/s².

In what follows, the vibration components in the stream, dam-axis and vertical directions are referred to as x-, y- and z-components, respectively, as shown in Figure 1, where the positive directions of those components are also indicated with arrows.

4 VIBRATION PERIODS OF THE DAM

First the vibration periods of the dam were analyzed using spectral ratios (or transfer functions) between the crest and gallery based on the earthquake records Nos. 1–4. The spectral ratios of the x- and y- components are shown in Figure 3, where the horizontal and vertical axes are vibration period and spectral ratio, respectively. The longest of the peak periods in the spectral ratios for the 1996 earthquakes are $T = 0.33$–0.35 s and $T = 0.32$–0.33 s for x- and y- components, respectively.

For the Aratozawa dam with $H = 74.4$ m, empirical equations for the fundamental period T (Okamoto 1984) yields $T = 0.37$ s and $T = 0.34$ s, for the stream and dam-axis directions, respectively. Since the longest peak periods of $T = 0.33$–0.35 s and $T = 0.32$–0.33 s for the 1996 earthquakes are consistent with the periods obtained from the equations, the longest peak periods are thought to be the fundamental period of the dam in each direction. On the other hand, for the main shock, the longest two peak periods are $T = 0.65$ s and 1.20 s for the x-component, and $T = 0.56$ s and 0.98 s for the y-component. These periods are significantly longer than the fundamental periods from the 1996 earthquakes, implying nonlinear response of the dam due to the main shock.

When it comes to the nonlinear response of the dam, it is natural to expect that the spectral ratio varies with time during the main shock. The time-varying spectral ratio can be obtained from a ratio of running spectra of the time histories observed at the dam crest and bottom gallery. The running spectral ratio was calculated with a temporal window of $\tau = 5.12$ s with the result shown in Figure 4, where the broken line in the darkest band indicates the most predominant period. The predominant period of the x-component was suddenly elongated to $T = 1.20$ s at around 4 s when the intense motion was input at the gallery, shortened again to $T = 0.65$ s at around 8.0 s when the intense motion started to decay, and finally approached $T = 0.5$ s. Likewise, the predominant period of the y-component was suddenly elongated to $T = 0.98$ s at around 4 s, shortened to $T = 0.56$ s, and finally approached $T = 0.4$ s.

Hence, both peak periods of $T = 0.65$ s and 1.20 s of the x-component, and $T = 0.56$ s and 0.98 s of the y-component are found to appear separately corresponding to the start and end of the intense motion input at the gallery, and are closely related to the fundamental vibration

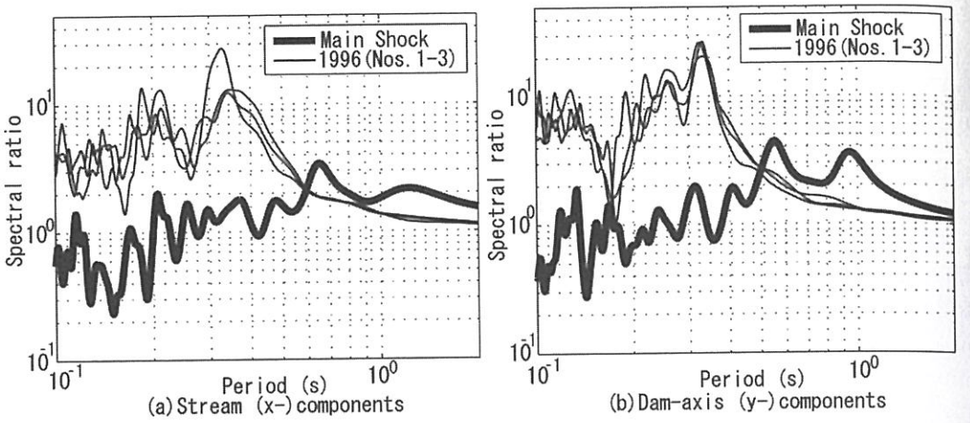

Figure 3. Spectral ratios between the crest and gallery.

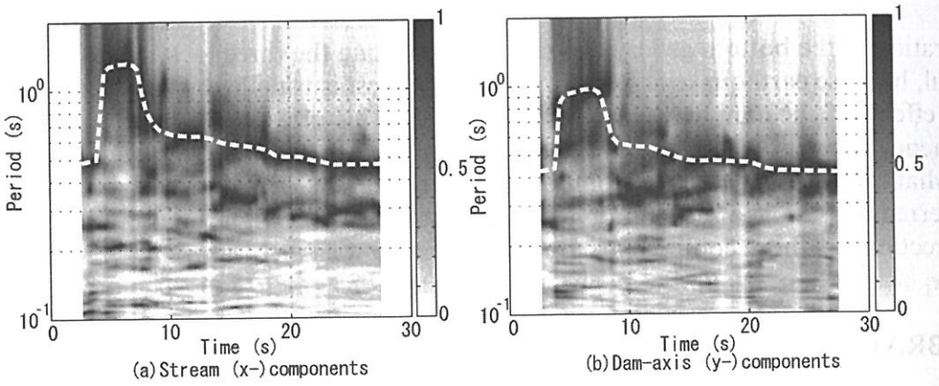

Figure 4. Running spectral ratios between the crest and gallery.

periods of the dam in both horizontal directions. Since the change in the vibration periods during the main shock implies a change in the seismic wave velocity within the dam body, the wave velocity will be discussed next.

5 ESTIMATION OF SEISMIC WAVE VELOCITY

The seismic wave velocity between a pair of the seismometers is estimated from the Fourier phase spectra of the acceleration time histories. When a seismic wave observed at seismometer A is propagated to seismometer B, the arrival time at seismometer B is delayed from that at seismometer A by $\Delta t = l/v$ where l is the distance between the two seismometers, and v is the wave velocity. With Fourier phase θ_A at seismometer A and θ_B at seismometer B, the phase difference $\theta = \theta_B - \theta_A$ is expressed as

$$\theta = 2\pi l / \lambda, \tag{1}$$

where λ is the wave length expressed as $\lambda = vT$ with period T. Substitution of $\lambda = v/f\,(=vT)$ in Eq. (1) leads to

$$\theta = 2\pi l f / v. \tag{2}$$

Hence, when the phase difference θ is plotted against the frequency f, the velocity v can be estimated from the slope of the plots.

Since the seismometers are installed at 3 locations on a vertical line (see Fig. 1), the wave velocity is estimated for the 3 sections shown in Table 2, where distances l of the sections are also shown. The stream (x-) component of the seismic wave velocity that is estimated from 1996 earthquakes is given in Table 3. All the estimated velocities seem to be reliable (Sawada & Takahashi 1975).

Table 2. Sections where wave velocity is estimated and their distance.

Section	Terminal observation points (A/B)	Distance l (m)
U	Mid-core/Dam-crest	29
M	Gallery/Dam-crest	75
L	Gallery/Mid-core	46

Table 3. Wave velocity of stream (x-) component from 1996 earthquakes.

	Section U (m/s)	Section M (m/s)	Section L (m/s)
Earthquake No. 1	429	496	564
Earthquake No. 2	424	487	565
Earthquake No. 3	435	501	573

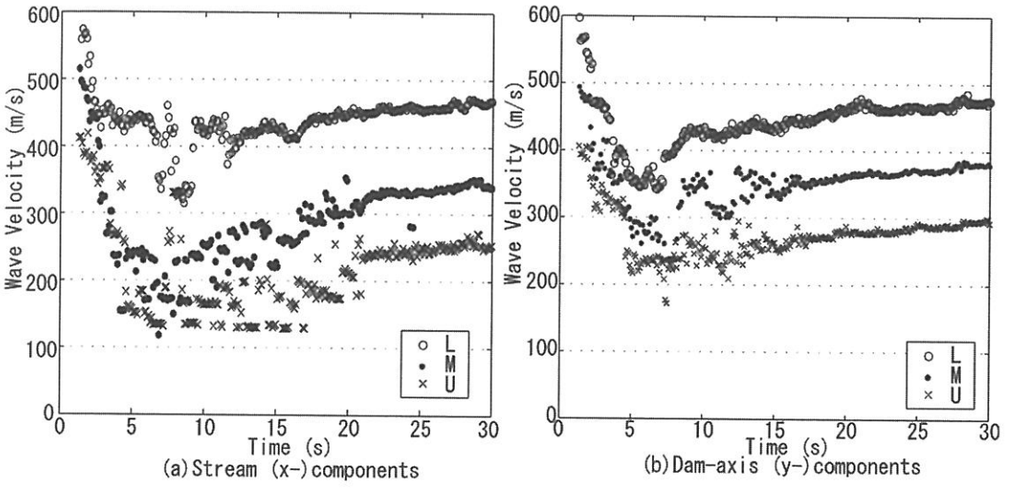

Figure 5. Wave velocities of 3 sections during main shock.

Using the same procedure, the seismic wave velocity during the main shock was estimated from Fourier phases of the acceleration time histories. Since the wave velocity was expected to change with time, the estimation procedure was applied in succession with a 2.56 s long moving temporal window. Figure 5 shows the time-varying wave velocities at the 3 sections estimated from the stream (x-) and dam-axis (y-) components, respectively. Although there is scatter in the estimated velocities, it can be observed that,

- Due to the intense shaking during the first 8 s, the wave velocities at all 3 sections showed a sudden decrease with time.
- The decrease in the velocity was more conspicuous in the upper part (section U) than in the lower part (section L) of the core zone.
- After the strong shaking, the wave velocity increased gradually with time.
- Initially both horizontal components at a particular section had the same velocity, but after the intense shaking, the stream (x-) component tended to exhibit a smaller velocity than the dam-axis (y-) component, especially for sections M and U.

6 STRAIN-DEPENDENCY OF DYNAMIC SOIL PROPERTIES

The acceleration time histories were integrated twice to obtain displacement histories. From the displacement time histories, relative displacements between the two ends of each section shown in Table 2 were obtained and divided by the distance between a pair of installations in order to calculate the mean shear strain of each section.

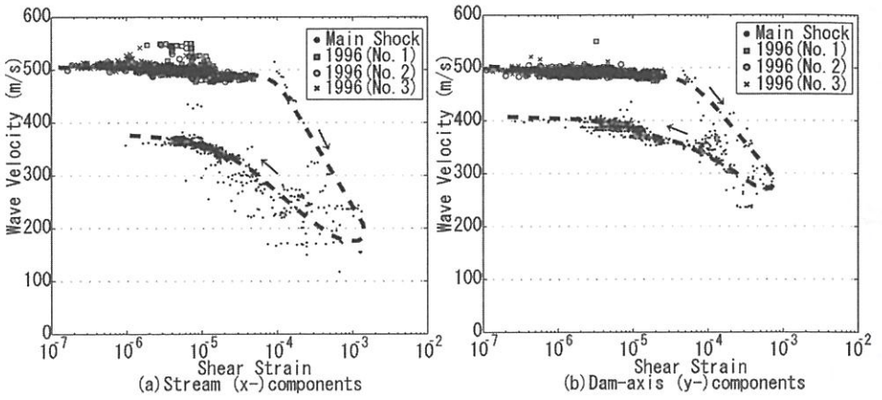

Figure 6. Strain-dependent wave velocity evaluated for horizontal components.

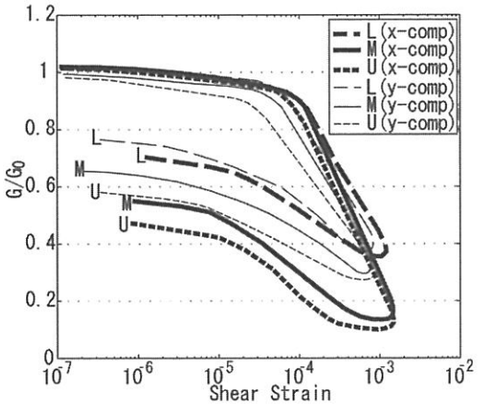

Figure 7. Strain-dependent shear modulus ratio.

Next the time-varying positive envelope of the mean shear strain which is regarded as a reference shear strain and the corresponding time-varying wave velocity shown in Figure 5 are plotted in Figure 6. In addition, the wave velocity-shear strain data from the 1996 earthquake records are also plotted, and an outline of the strain history during the main shock is shown with a dashed line and arrows. In Figure 6, when the shear strain exceeds 10^{-4}, the shear wave velocity shows a sudden decrease, and then increases again with the decrease in the strain level.

It is assumed that the shear wave velocity V_S and the shear modulus G are related by,

$$V_S = (G / \rho)^{1/2} \tag{3}$$

where ρ is mass density. As the change in mass density is negligibly small in comparison with the change in shear modulus, the above mentioned strain-dependent wave velocity V_S is converted to a strain-dependent shear modulus G, as shown in Figure 7 in which G_0 denotes the initial shear modulus at low strain. It should be noted in Figures 6 and 7 that at the end of the main shock the shear wave velocity V_S and shear modulus G remained considerably smaller than their initial values. In Figure 7, the six lines associated with the gradual increase are almost parallel to each other. Due to the parallel increase in the ratio G/G_0, the modulus G in the core becomes anisotropic during the increasing process including the final state.

7 LONG-TERM RECOVERY OF DECREASED WAVE VELOCITY AND ISOTROPY

Acceleration time histories of 185 earthquake events at the dam which were recorded after the main shock of the 2008 earthquake were analyzed. Among these events, the largest peak acceleration recorded at the gallery was 4.82 m/s^2 corresponding to event No. 6 which was an aftershock occurring 18 minutes after the main shock (see Table 1).

The recovery process of the decreased wave velocity was investigated, with the result shown in Figure 8 for section M. It can be said that, in general the decreased wave velocities have almost recovered to the initial values by August, 2009, and the anisotropy in the wave velocity has also disappeared by then.

8 PORE WATER PRESSURE BEFORE AND AFTER MAIN SHOCK

The pore water pressure distribution in a vertical section was estimated from daily readings of the meters at 9:00 AM before and after the main shock, as shown in Figure 9 where small circles

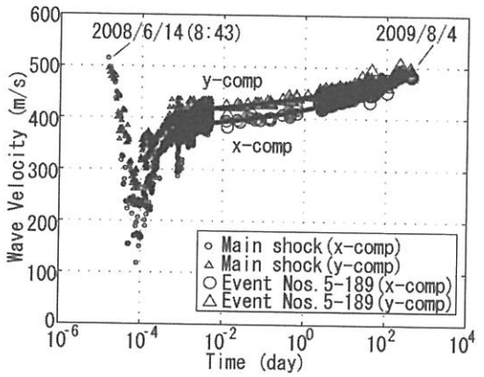

Figure 8. Long-term recovery of the decreased wave velocity and isotropy of section M.

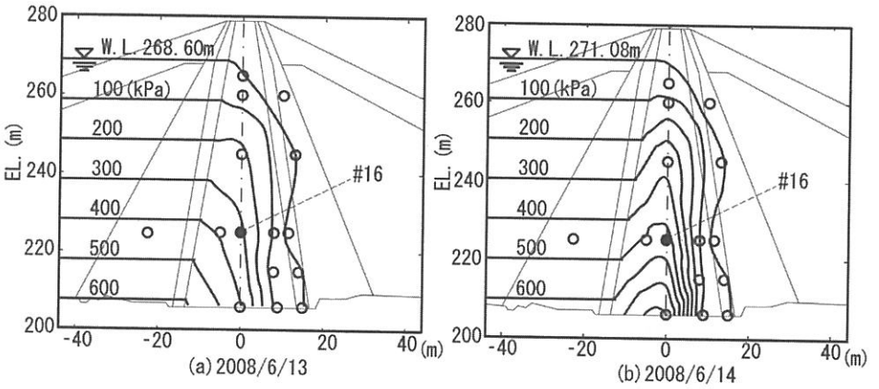

Figure 9. The generation and dissipation of excess pore water pressure in the core. Small circles indicate location of pore water pressure meters. The solid circle indicates the location of pore water pressure meter #16.

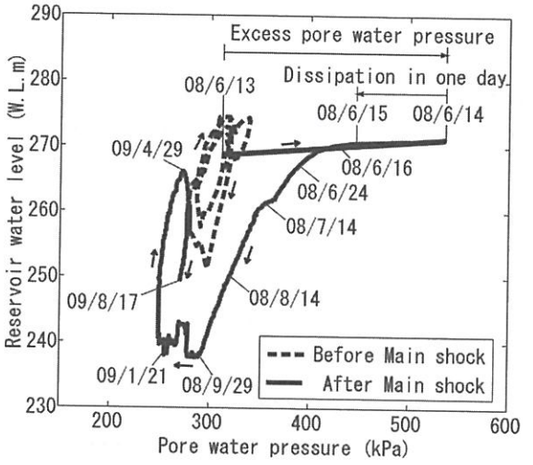

Figure 10. Time history of pore water pressure at meter #16.

indicate locations of the meters and a simple distribution is assumed on the upstream side. The section is the cross section A-A' shown in Figure 1(b) where the seismometers are installed.

The pore water pressure of June 13, 2008 (denoted by 2008/6/13) was distributed in the typical pattern of a normal steady state condition, although the estimated phreatic line was not so smooth as expected, maybe due to some mechanical errors included in the readings. On June 14, seventeen minutes after the main shock, the distribution pattern had changed to exhibit a sudden build-up of excess pore water pressure especially at the lower part of the core zone, while the build-up was not so obvious in the other zones such as filter and transition zones.

Figure 10 shows a series of the daily readings of the pore water pressure meter #16 whose location is shown with a solid circle at EL.225 m in Figure 9. It can be seen that after the main shock, with a continuous drawdown of the reservoir water level to W.L.237.7 m, the pore water pressure showed a monotonous decrease. The readings on June 13, 14 and 15 were 314, 535 and 442 kPa, respectively. Hence, the excess pore water pressure produced by the main shock was dissipated by 42% within a single day after the main shock. The dissipation of the excess pore water pressure seems faster than the long-term recovery of the decreased wave velocity.

9 CONCLUSIONS

Conclusions drawn from the present study are:

- During the main shock of the 2008 earthquake, the acceleration of the stream component exceeded 10 m/s^2 at the gallery, but did not exceed 5.3 m/s^2 at the dam crest.
- The intense shaking of the main shock induced large shear strains in excess of 10^{-3} in the stream direction and a little below 10^{-3} in the dam-axis direction.
- Due to the large strains in the horizontal directions, the shear modulus G exhibited a remarkable decrease from the initial shear modulus G_0 by 90% in the upper part and 60% in the lower part of the core.
- As a result of the decrease in G, the shear wave velocity V_S in the core was significantly reduced and the fundamental period of the dam was elongated to $T = 1.20$ s, which lead to the attenuation of the earthquake response of the dam.
- Towards the end of the main shock, the modulus G in the core showed a gradual increase, but remained below G_0 and was anisotropic.
- The decreased shear wave velocity continued to recover and the anisotropy decreased with the passage of time, and the full recovery of the wave velocity to the initial one of isotropy was found to take at least one year.
- During the main shock, excess pore water pressure was also induced in the core. The dissipation of the excess pore water pressure seemed faster than the recovery of the decreased wave velocity.

ACKNOWLEDGEMENTS

The authors would like to express their thanks to the civil engineers in Miyagi Prefecture for providing information about earthquake response of the Aratozawa dam.

REFERENCES

Japan Meteorological Agency. 2008. Iwate-Miyagi Nairiku earthquake in 2008. http://www.seisvol.kishou.go.jp/eq/2008_6_14_iwate-miyagi/index.html

Okamoto, S. 1984. Earthquake resistance of embankment dams. *Introduction to Earthquake Engineering 2nd Edition*. Japan: University of Tokyo Press.

Sawada, Y. & Takahashi, T. 1975. Study on the material properties and the earthquake behavior of rockfill dams. *Proc. 4th Japan Earthquake Engineering Symposium*: 695–702.